Fiber gyro with squeezed radiation

H. A. Haus, K. Bergman, and Y. Lai

Department of Electrical Engineering and Computer Science and Research Laboratory of Electronics, Massachusetts Institute of Technology, Cambridge, Massachusetts 02139

Received December 11, 1990; revised manuscript received April 30, 1991

A pulse-excited Sagnac fiber interferometer can perform squeezing. If this squeezed radiation is injected into a second Sagnac interferometer that is functioning as a fiber gyro that is itself nonlinear, additional unfavorable squeezing occurs in the gyro. By proper phase adjustment of the injected squeezed radiation it is possible to minimize this effect as long as the Sagnac interferometer that is performing the squeezing has a sufficiently large nonlinearity.

1. INTRODUCTION

Squeezing in a fiber ring by using a pulsed pump was recently accomplished with a surprising degree of success.[1] Previous fiber squeezing experiments with quasi-cw excitation[2,3] were subject to low stimulated Brillouin scattering thresholds and to guided-acoustic-wave Brillouin scattering.[4] The pulsed excitation avoids stimulated Brillouin scattering. The Sagnac-ring configuration used in Ref. 1 separates the pump radiation from the squeezed radiation and therefore permits observation at low (40 kHz) frequencies, because pump noise fluctuations do not accompany the squeezed radiation. Guided-acoustic-wave Brillouin scattering does not affect the squeezed radiation at low frequencies.

The separation of the pump from the squeezed radiation has the other advantage that no power need be wasted in the squeezing process. All the pump power can, in principle, be reused as the signal in a Sagnac-ring fiber gyro. This use may be the first practical application of the new squeezing scheme. Before one can employ the scheme, however, several issues must be addressed. As we explain below, the nonlinearity in the fiber gyro produces squeezing of its own but in an unfavorable direction. The question then is how nonlinear the fiber gyro can be before the beneficial effect of the squeezed radiation injected into its vacuum port is lost. Further, it is not yet known whether the nonlinearities of the fiber, enhanced by the use of pulsed radiation, will pose problems that are not encountered with (quasi-) cw-excited fiber gyros.

In the present paper we briefly review the squeezing operation of a fiber ring. Then we outline a design for a fiber gyro in cascade with the squeezing ring. We show how the shot-noise-limited signal-to-noise ratio of the gyro can be overcome with squeezed radiation injected into the vacuum port of the gyro when the gyro can be considered to be linear. Since both the squeezing ring and the fiber gyro use comparable fiber lengths, nonlinearities in the gyro are unavoidable, if it is assumed that the same intensity pulses are used in both. This is, of course, the desirable method of operation, since otherwise the good signal-to-noise ratio would be sacrificed. Finally, we establish limits on the nonlinearity of the fiber gyro such that the decrease in the signal-to-noise ratio is made acceptable.

2. FIBER RING SQUEEZER

Figure 1 shows the fiber ring squeezer that is used in the experiment in pulse squeezing. Its operation is best understood by replacing the ring reflector with the equivalent nonlinear Mach–Zehnder interferometer of Fig. 2. The two systems are equivalent when the small interaction of the two countertraveling pulses in the ring of Fig. 1 is neglected. Of course, the ring has the advantage of being self-stabilized with regard to slow fluctuations in temperature, stress, etc. that affect the pulse by their associated index changes.

In the slowly varying envelope approximation, quantization of pulsed radiation is equivalent to quantization of square segments of the pulse as if they were cw waves.[5] This approximation is valid as long as dispersion may be neglected and each time segment considered independently. Then consider one segment of the pulse, as shown in Fig. 2, and the cotraveling zero-point fluctuations of the vacuum input port within the same time slot. These can be represented by phasors in the phasor plane and the associated Wigner distribution (probability distribution of mean-square fluctuations plotted along their respective phase directions). The phasors, corresponding to the pump $\hat{f}_p$ and the (coherent) zero-point fluctuations $\hat{a}$, are shown next to the time functions. After the 50/50 beam splitter, the noise fluctuations in the two arms are still uncorrelated. If the analysis is linearized in terms of the fluctuation (operator) amplitudes, the propagation of the phasors through their respective Kerr media results in a distortion of the Wigner distribution from circles (representing the locus of half-power points) into ellipses, which are tangent to the vertical tangents as shown. This distortion occurs because different input amplitudes result in different Kerr phase shifts. In the graphs we suppress the common Kerr phase shift that is imposed on the signal and the noise. At the output beam splitter the phasors add at one output port and subtract at the other. The squares of the uncorrelated noise fluctuations, of course,

0740-3224/91/091952-06$05.00

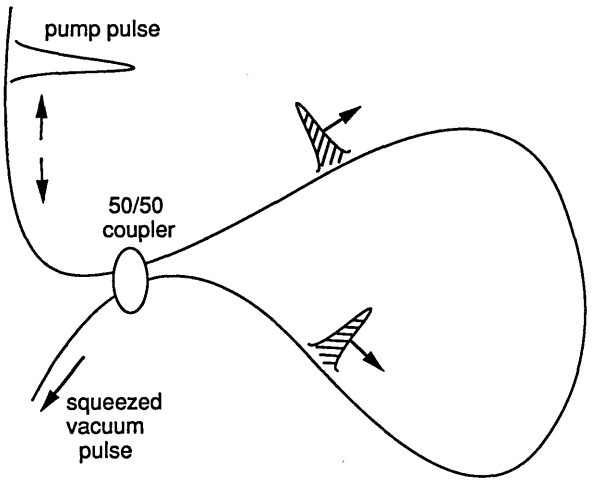

Fig. 1. Fiber ring squeezer.

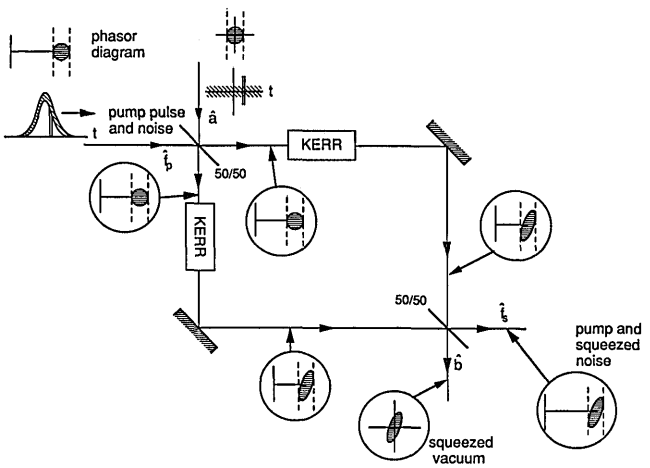

Fig. 2. Equivalent Mach–Zehnder squeezer.

add. The two half-pump amplitudes thus subtract at the vacuum output port, resulting in separation of the pump and the squeezed radiation. This is the operating principle of the Sagnac-ring squeezer.

3. RING SQUEEZER AND RING FIBER GYRO IN CASCADE

Consider next the Sagnac-ring squeezer discussed above in cascade with a fiber ring gyro. For the moment assume that the fiber gyro is linear. We present the schematic by using the equivalent Mach–Zehnder interferometer in Fig. 3. In the fiber ring configuration the input and the output ports are physically identical. In order to separate the outcoming pump from the ingoing pump, we need a nonreciprocal coupler that transmits all the forward-traveling wave and fully cross-couples the backward-traveling wave. A similar isolation has to be provided for the vacuum ports.

Figure 3 shows the progress of the signal and the noise through the system. The squeezer prepares the squeezed radiation (designated by the operator amplitude $\hat{b}$) in one output port; the pump (designated by the operator $\hat{f}_s$) emerges from the other output port. The phase shifter reorients the principal axes. This squeezed radiation enters the Sagnac gyro. The pump of the first ring is used as the signal that is injected into the gyro. The phase shifts in the two arms are not identical, because of the Sagnac effect, and a net signal emerges in the vacuum output port of the gyro. This net signal is the gyro signal to be measured. (We have assumed that the squeezing ring experiences no Sagnac effect. This condition can be met by proper winding of the fiber ring.) Because squeezed radiation has been injected into the vacuum port of the gyro, the in-phase noise of the signal is reduced. The balanced homodyne detector sees a signal accompanied by a noise that is smaller than shot noise. Standard zero-point fluctuations entering the vacuum port of the gyro would yield shot noise.

In this simple picture we ignore the effect of the Sagnac imbalance of the gyro on the noise. This is the usual approximation that ignores signal-dependent noise.

The preceding discussion shows clearly why the operation of squeezing and that of the Sagnac gyro measurement has to be separated into two rings. The squeezing produces an ellipse with a major axis of orientation that tends toward perpendicularity with respect to the pump phasor. If the pump is used as the Sagnac signal source and noise reduction is to be achieved, the major axis has to be rotated parallel to its phasor.

Next, consider the case when the gyro itself is a nonlinear Mach–Zehnder interferometer. The pulse will do its own squeezing, in the wrong direction, as we explained earlier. However, some of the effect can be counterbalanced, as was pointed out in the context of a quantum nondemolition measurement.[6] The analysis is in fact quite simple if one takes advantage from the start of an important property of the balanced nonlinear Mach–Zehnder interferometer. It turns out that with the linearization approximation the noise fluctuations entering either arm are squeezed independently.[7] Therefore we need solely to follow the fate of the squeezed vacuum input through the gyro in order to ascertain the effect of the gyro nonlinearity on the noise. Figure 4 shows the system again but with a nonlinear gyro. The inset in Fig. 4 illustrates how one must prepare the squeezed vacuum to counterbalance, in part, the effect of the gyro nonlinearity. The major axis of the ellipse of the squeezed vacuum input has to be inclined by an appropriate negative angle.

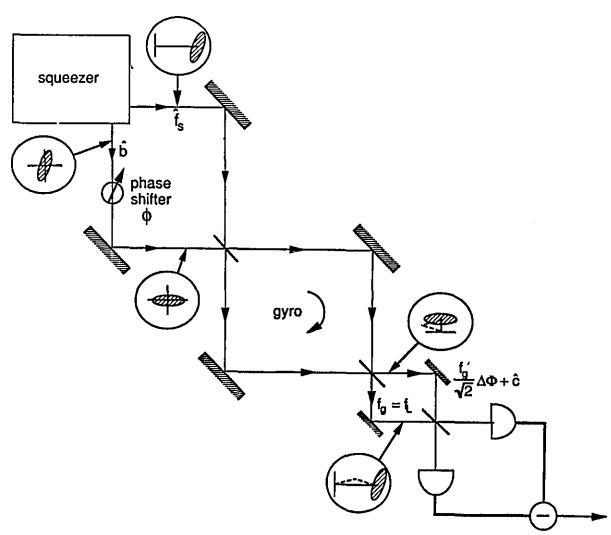

Fig. 3. Squeezer followed by a gyro.

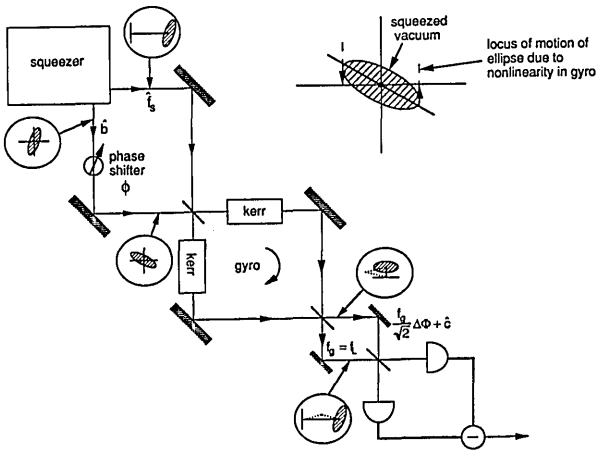

Fig. 4. Squeezer followed by a nonlinear gyro, with squeezed vacuum preparation at input to gyro.

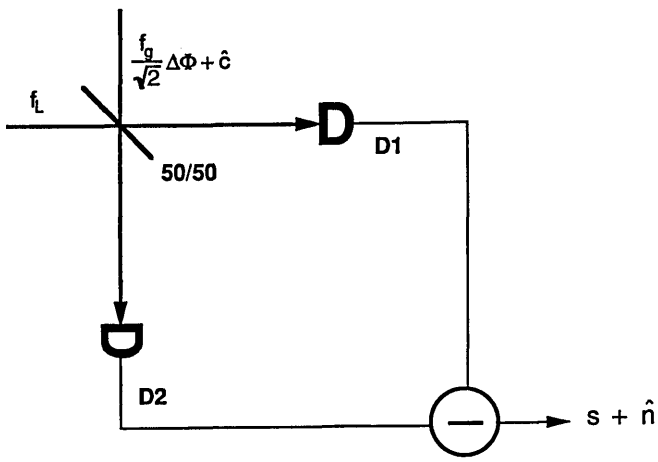

Fig. 5. Schematic of the homodyne detection.

As the fluctuations pass through the interferometer, the nonlinearity will shift the fluctuations that are in phase with the signal more than those in quadrature, resulting in an output with a horizontal major axis. We present the analysis in Sections 4 and 5.

4. SIGNAL-TO-NOISE RATIO

In this section we calculate the signal-to-noise ratio for cw (not pulse) excitation of our gyro setup following a homodyne detection. The configuration of homodyne detection is shown in Fig. 5. A local oscillator field with the annilhilation operator $\hat{f}_L$ is mixed with the gyro signal, $f_g\Delta\phi/\sqrt{2}$, and its accompanying noise, $\hat{c}$, through a 50/50 beam splitter. The output currents of the two photodetectors are subtracted in order to suppress the fluctuation from the local oscillator. Here f_g is the output pump of the gyro, and $\Delta\phi$ is rotation-induced phase imbalance. The separated noise component $\hat{c}$ is the lowest-order noise that would be encountered in a balanced interferometer. We ignore the higher-order noise term that arises from the Sagnac imbalance. This term is proportional to $\Delta\phi$ and is of much smaller magnitude than $\hat{c}$. The noise operator $\hat{c}$ obeys the following commutation relation:

$$[\hat{c}, \hat{c}^\dagger] = 1. \tag{4.1}$$

The operation of homodyne detection is described compactly by means of the following vector notation. By definitions

$$\hat{\mathbf{f}}_\mathbf{L} = \begin{bmatrix} \hat{f}_{L1} \\ \hat{f}_{L2} \end{bmatrix}, \tag{4.2}$$

$$\mathbf{f}_\mathbf{g} = \begin{bmatrix} f_{g1} \\ f_{g2} \end{bmatrix}, \tag{4.3}$$

$$\hat{\mathbf{c}} = \begin{bmatrix} \hat{c}_1 \\ \hat{c}_2 \end{bmatrix}, \tag{4.4}$$

with subscripts 1 and 2 indicating the real and imaginary parts, respectively, the operation of homodyne detection is simply the projection of the incoming optical field into the local oscillator field. The output of the homodyne detection consequently becomes

$$s + \hat{n} \equiv \frac{\mathbf{f_L}^T\mathbf{f_g}\Delta\phi}{\sqrt{2}} + \mathbf{f_L}^T\hat{\mathbf{c}}, \tag{4.5}$$

where the superscript T indicates a transpose. The first term in Eq. (4.5) is the signal term, and the second term is the noise term. We have also replaced $\mathbf{f_L}$ by its c-number expectation value, thereby ignoring the noise of the local oscillator compared with the amplified (squeezed) zero-point fluctuation. The signal power is given by

$$S = |s|^2 = \tfrac{1}{2}|\mathbf{f_L}^T\mathbf{f_g}|^2(\Delta\phi)^2, \tag{4.6}$$

and the noise power is given by

$$N = \langle\hat{n}^2\rangle = \mathbf{f_L}^T\mathbf{C}(\hat{\mathbf{c}})\mathbf{f_L}. \tag{4.7}$$

Here

$$\mathbf{C}(\hat{\mathbf{c}}) \equiv \tfrac{1}{2}\langle\hat{\mathbf{c}}\hat{\mathbf{c}}^\mathbf{T} + (\hat{\mathbf{c}}\hat{\mathbf{c}}^\mathbf{T})^\mathbf{T}\rangle \tag{4.8}$$

is the symmetrized correlation matrix of the operator vector $\hat{\mathbf{c}}$. For a coherent state the correlation matrix is $\mathbf{I}/4$ with $\mathbf{I}$ being the identity matrix, and thus its noise power is

$$N_c = \tfrac{1}{4}\mathbf{f_L}^T\mathbf{f_L}. \tag{4.9}$$

This is the shot-noise level.

To simplify the expressions, we define

$$S_L \equiv \mathbf{f_L}^T\mathbf{f_L}, \tag{4.10}$$

$$S_g \equiv \mathbf{f_g}^T\mathbf{f_g}, \tag{4.11}$$

where S_L is the local oscillator power and S_g is the output pump power of the gyro. We now define F, the matching factor between the signal and the local oscillator ($0 \le F \le 1$), as

$$F \equiv \frac{|\mathbf{f_L}^T\mathbf{f_g}|^2}{S_L S_g}. \tag{4.12}$$

When $\mathbf{f_L} \propto \mathbf{f_g}$ the local oscillator and the signal are perfectly matched and $F = 1$. In the present (cw) case, perfect matching is achieved simply by equating the phases of f_L and f_g. The squeezing reduction factor R is defined as the ratio between the noise power N to the shot-noise power N_c,

$$R \equiv \frac{N}{N_c} = \frac{\mathbf{f_L}^T\mathbf{C}(\hat{\mathbf{c}})\mathbf{f_L}}{\tfrac{1}{4}S_L}. \tag{4.13}$$

With the above notations each of the expressions for S, N, and S/N (signal-to-noise ratio) can be put into a simpler form:

$$S = \tfrac{1}{2}FS_L S_g(\Delta\phi)^2, \tag{4.14}$$

$$N = \tfrac{1}{4}S_L R, \tag{4.15}$$

$$S/N = \frac{2FS_g}{R}(\Delta\phi)^2. \tag{4.16}$$

From Eq. (4.16) it is immediately apparent that the reduction factor $R(<1)$ will increase the signal-to-noise ratio. We proceed with the analysis to determine R.

5. ANALYSIS OF THE NONLINEAR GYRO

By choosing the phase of the outgoing pump as the phase reference, the squeezed vacuum emerging from the squeezing ring is described by the operator[6]

$$\hat{b} = \mu_0\hat{a} + \nu_0\hat{a}^\dagger, \tag{5.1}$$

where

$$\mu_0 = 1 + i\Phi_s, \qquad \nu_0 = i\Phi_s, \tag{5.2}$$

and Φ_s is the nonlinear phase shift in the squeezer and is related to the Kerr coefficient n_2, wavelength λ, fiber length l, and intensity I inside the fiber by

$$\Phi_s = \frac{2\pi}{\lambda}n_2 l\frac{I}{\mathcal{A}_{\text{eff}}}. \tag{5.3}$$

Here $\mathcal{A}_{\text{eff}}$ is the effective area of the fiber. The operator $\hat{b}$ is shifted by phase ϕ by means of the phase shifter and then squeezed by the gyro with squeezing parameters $\mu_g = 1 + i\Phi_g$ and $\nu_g = i\Phi_g$. Here Φ_g is the nonlinear phase shift in the gyro.

Written in vector form, one has

$$\hat{\mathbf{b}} = \mathbf{M}_0\hat{\mathbf{a}}, \tag{5.4}$$

where, from Eqs. (5.1) and (5.2), the squeezing matrix $\mathbf{M}_0$ is given by

$$\mathbf{M}_0 = \begin{bmatrix} 1 & 0 \\ 2\Phi_s & 1 \end{bmatrix}. \tag{5.5}$$

The correlation matrix of the output of the squeezer is

$$\begin{aligned} \mathbf{C}(\hat{\mathbf{b}}) &= \mathbf{M}_0\mathbf{C}(\hat{\mathbf{a}})\mathbf{M}_0^{\mathrm{T}} \\ &= \frac{1}{4}\mathbf{M}_0\mathbf{M}_0^{\mathrm{T}} \\ &= \frac{1}{4}\begin{bmatrix} 1 & 2\Phi_s \\ 2\Phi_s & 1 + 4\Phi_s^2 \end{bmatrix}. \end{aligned} \tag{5.6}$$

The maximum and minimum mean-square fluctuations are the eigenvalues of the correlation matrix obtained from the determinantal equation

$$\det[\mathbf{C}(\hat{\mathbf{b}}) - \lambda\mathbf{I}] = 0. \tag{5.7}$$

They are found to be

$$\lambda = \tfrac{1}{4}[1 + 2\Phi_s^2 \pm 2\Phi_s(1 + \Phi_s^2)^{1/2}]. \tag{5.8}$$

It is easily confirmed that these values are the familiar ones obtained from the squeezing parameters μ_0 and ν_0:

$$\lambda = \tfrac{1}{4}(|\mu_0| \pm |\nu_0|)^2, \tag{5.9}$$

where

$$|\mu_0| = (1 + \Phi_s^2)^{1/2}, \qquad |\nu_0| = \Phi_s. \tag{5.10}$$

We now proceed further through the system. After the gyro the operator vector $\hat{\mathbf{c}}$ is produced according to the law

$$\hat{\mathbf{c}} = \mathbf{M}_g\mathbf{R}(\phi)\hat{\mathbf{b}}, \tag{5.11}$$

where $\mathbf{R}(\phi)$ is a simple rotation of a phase angle ϕ caused by the phase shifter and $\mathbf{M}_g$ is the matrix (5.5) with Φ_s replaced by the nonlinear phase Φ_g of the gyro. Since we always choose the phase of the outgoing pump as the phase reference, the gyro signal is pure imaginary. To detect the maximum signal, one has to put all the local oscillator power into the imaginary part:

$$\mathbf{f}_{\mathrm{L}} = \begin{bmatrix} 0 \\ 1 \end{bmatrix}. \tag{5.12}$$

Here again we treat the local oscillator field as a c number, ignoring the noise of the local oscillator compared with the (homodyne) amplified (squeezed) zero-point fluctuations. From Eq. (4.6) the noise power is given by

$$\begin{aligned} N &= [0,1]\mathbf{C}(\hat{\mathbf{c}})\begin{bmatrix} 0 \\ 1 \end{bmatrix} \\ &= [0,1]\mathbf{M}_g\mathbf{R}(\phi)\mathbf{C}(\hat{\mathbf{b}})\mathbf{R}^{\mathrm{T}}(\phi)\mathbf{M}_g^{\mathrm{T}}\begin{bmatrix} 0 \\ 1 \end{bmatrix}. \end{aligned} \tag{5.13}$$

Let us study in more detail the matrix premultipliers and postmultipliers. The premultiplier is

$$[0,1]\mathbf{M}_g = [2\Phi_g, 1] = (1 + 4\Phi_g^2)^{1/2}[0,1]\mathbf{R}(-\theta), \tag{5.14}$$

where the angle θ is determined by

$$\sin\theta = \frac{2\Phi_g}{(1 + 4\Phi_g^2)^{1/2}}, \tag{5.15}$$

$$\cos\theta = \frac{1}{(1 + 4\Phi_g^2)^{1/2}}. \tag{5.16}$$

In the development of Eq. (5.17) we recognize that the operation can be written as the product of a rotation by angle θ, a projection, and $(1 + 4\Phi_g^2)^{1/2}$. With the aid of the above vector formalism, one may write the noise

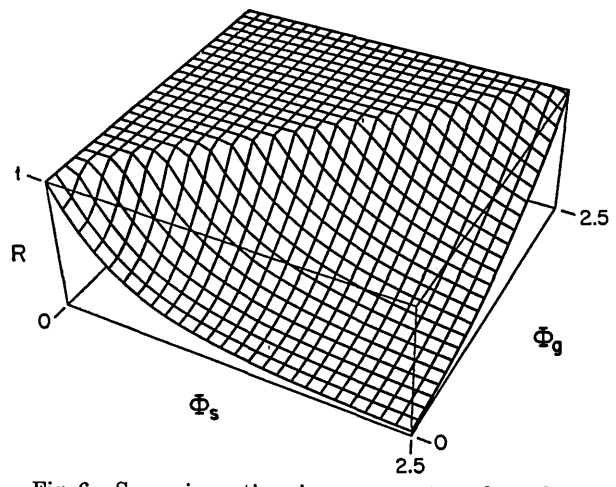

Fig. 6. Squeezing ratio using cw or rectangular pulses.

power as

$$N = (1 + 4\Phi_g^2)[0,1]\mathbf{R}(-\theta)\mathbf{R}(\phi)\mathbf{C}(\hat{\mathbf{b}})\mathbf{R}^T(\phi)\mathbf{R}^T(-\theta)\begin{bmatrix}0\\1\end{bmatrix}. \tag{5.17}$$

In this form it is easy to recognize the result. The product $\mathbf{R}(\phi)\mathbf{R}(-\theta)$ is simply a rotation that does not change the eigenvalues. By adjusting the value of ϕ, one can diagonalize the matrix to bring the smaller of the two eigenvalues to position 22 of the matrix. When this diagonalization is done, the mean square fluctuations are minimized to the smaller of the two values of (5.8). The squeezing reduction factor R is thus given by

$$R \equiv \frac{\min_\phi\left\{[0,1]\mathbf{M}_g\mathbf{R}(\phi)\mathbf{C}(\hat{\mathbf{b}})\mathbf{R}^T(\phi)\mathbf{M}_g{}^T\begin{bmatrix}0\\1\end{bmatrix}\right\}}{\frac{1}{4}}$$

$$= (1 + 4\Phi_g^2)[1 + 2\Phi_s^2 - 2\Phi_s(1 + \Phi_s^2)^{1/2}]. \tag{5.18}$$

It is clear that $(1 + 4\Phi_g^2)$ is the penalty factor that is due to the nonlinearity in the fiber gyro. If the noise is not to be greatly enhanced, this factor must be kept close to unity, or $4\Phi_g^2 \ll 1$. This can be seen in Fig. 6, where the squeezing ratio from (5.18) is plotted as a function of Φ_s and Φ_g. Equation (5.18) holds for cw and rectangular pulses.

To obtain the overall squeezing ratio for nonrectangular pulses (i.e., Gaussian pulses), one has to average the squeezing reduction across the whole pulse duration and weigh the average by the local oscillator intensity:

$$R \equiv \frac{\min_\phi\left\{\int [0, f_L(t)]\mathbf{M}_g\mathbf{R}(\phi)\mathbf{C}[\hat{\mathbf{b}}(t)]\mathbf{R}^T(\phi)\mathbf{M}_g{}^T\begin{bmatrix}0\\f_L(t)\end{bmatrix}dt\right\}}{\frac{1}{4}\int |f_L(t)|^2 dt}$$

$$= \frac{\min_\phi\left(\int |f_L(t)|^2[1 + 4\Phi_g^2(t)]\{1 + 2\Phi_s^2(t) + 2\Phi_s(t)[1 + \Phi_s^2(t)]^{1/2}\cos[2\phi - 2\theta(t) - \gamma(t)]\}dt\right)}{\int |f_L(t)|^2 dt}$$

$$= \frac{\int |f_L(t)|^2[1 + 4\Phi_g^2(t)]\{1 + 2\Phi_s^2(t) - 2\Phi_s(t)[1 + \Phi_s^2(t)]^{1/2}\cos[2\theta(0) + \gamma(0) - 2\theta(t) - \gamma(t)]\}dt}{\int |f_L(t)|^2 dt}. \tag{5.19}$$

Here $f_L(t)$ is the local oscillator pulse shape and $\gamma(t)$ is defined in terms of

$$\sin[\gamma(t)] = \frac{1}{[1 + \Phi_s^2(t)]^{1/2}}, \tag{5.20}$$

$$\cos[\gamma(t)] = \frac{\Phi_s(t)}{[1 + \Phi_s^2(t)]^{1/2}}. \tag{5.21}$$

Since the pump pulse from the gyro is also the local oscillator, $|f_L(t)|^2 \propto \Phi_s(t) \propto \Phi_g(t)$. Equation (5.19) is a general result for any pulse shape. The cw case solution may be obtained by simply substituting a rectangular pulse shape for $f_L(t)$.

The result from (5.19) is plotted in Fig. 7 for the case of a Gaussian local oscillator and can be understood as follows. Both the squeezing magnitude and the squeezing direction are functions of the intensity. Therefore for nonrectangular pulses the squeezing direction varies across the pulse duration. Since we adjust the relative phase only by the constant ϕ, the best we can do is to choose ϕ such that the noise contribution from the peak is minimized. However, the mismatch of squeezing and detection directions also limits the achievable minimum-squeezing ratio to ~7 dB and makes the overall squeezing more sensitive to the nonlinearity in the gyro loop.

One way to get around this problem is by shaping the phase of the local oscillator pulse to match the squeezing direction across the whole pulse duration. By this technique the optimum squeezing ratio can be achieved, but the overall matching factor F is also reduced because the local oscillator does not match the signal perfectly.

Another way to avoid this problem is to work in the negative dispersion region (i.e., 1.5 μm) and to use solitons

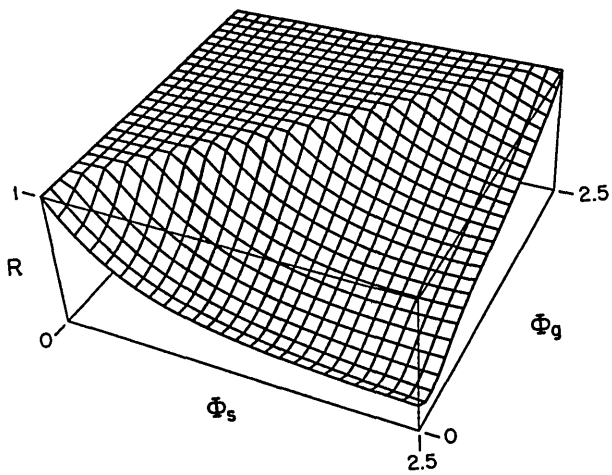

Fig. 7. Squeezing ratio using Gaussian pulses.

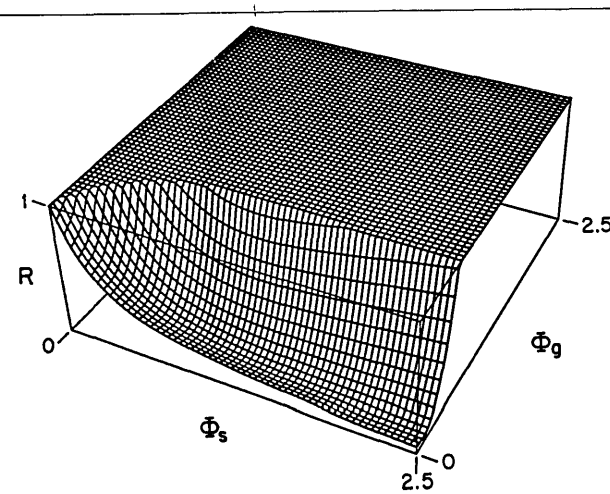

Fig. 8. Squeezing ratio using solitons.

The nonlinear phase of a soliton is constant across the whole pulse. The performance of such a soliton gyro is shown in Fig. 8. Compared with the case with Gaussian pulses, the achievable squeezing ratio is improved. However, compared with the case with rectangular pulses, the effect of the nonlinearity in the gyro loop is more severe.

6. CONCLUSIONS

We have shown that the nonlinearity in the fiber gyro worsens the signal-to-noise ratio by increasing the noise level to higher than the squeezing level of the squeezer. The noise doubles when the phase Φ_g acquired by the pulse in the gyro is equal to 0.5 rad. For the achievement of good squeezing, on the other hand, the phase shift in the squeezer must be greater than π. Thus the ratio of nonlinearities in the two fibers must be of the order of ≥ 6. The simplest way of implementing such a ratio would be by making the squeezing fiber six times longer than the gyro fiber. It is not clear whether that is feasible, because classical noises may become dominant if the squeezing fiber is too long. Another way would be to use fibers of different core diameters for the two rings. This method could be exploited only to a limited degree, since single-mode operation is required. The details of the design will have to await further study. The present investigation has clarified one of the effects of the nonlinearity in a fiber gyro using squeezed radiation.

ACKNOWLEDGMENTS

We are grateful to Draper Laboratories for supporting this research with grant DL-H-404179. The investigation was also supported in part by National Science Foundation grant EET-8700474.

REFERENCES

1. K. Bergman and H. A. Haus, "Squeezing in fibers with optical pulses," Opt. Lett. **16,** 663 (1991).
2. R. M. Shelby, M. D. Levenson, S. H. Perlmutter, R. G. DeVoe, and D. F. Walls, "Broad-band parametric deamplification of quantum noise in an optical fiber," Phys. Rev. Lett. **57,** 691 (1986).
3. R. M. Shelby, M. D. Levenson, D. F. Walls, A. Aspect, and G. J. Milburn, "Generation of squeezed states of light with a fiber-optic ring interferometer," Phys. Rev. A **33,** 4008 (1986).
4. R. M. Shelby, M. D. Levenson, and P. W. Bayer, "Guided acoustic-wave Brillouin scattering," Phys. Rev. B **31,** 5244 (1985).
5. M. Shirasaki and H. A. Haus, "Squeezing of pulses in a nonlinear interferometer," J. Opt. Soc. Am. B **7,** 30 (1990).
6. M. Shirasaki and H. A. Haus, "Noise reduction in quantum nondemolition measurement with a nonlinear Mach–Zehnder interferometer using squeezed vacuum," J. Opt. Soc. Am. B **8,** 681 (1991).
7. H. A. Haus, K. Watanabe, and Y. Yamamoto, "Quantum-nondemolition measurement of optical solitons," J. Opt. Soc. Am. B **6,** 1138 (1989).